The Journal of Chemical Physics

Line-shape theory of the $X^3\Sigma_g^- \rightarrow a^1\Delta_g, b^1\Sigma_g^+$ transitions in O_2–O_2 collision-induced absorption

Cite as: J. Chem. Phys. **147**, 084307 (2017); https://doi.org/10.1063/1.4990662
Submitted: 16 June 2017 . Accepted: 27 July 2017 . Published Online: 31 August 2017

Tijs Karman, Ad van der Avoird, and Gerrit C. Groenenboom

Line-shape theory of the $X^3\Sigma_g^- \rightarrow a^1\Delta_g, b^1\Sigma_g^+$ transitions in O_2–O_2 collision-induced absorption

Tijs Karman, Ad van der Avoird, and Gerrit C. Groenenboom[a)]
Theoretical Chemistry, Institute for Molecules and Materials, Radboud University, Heyendaalseweg 135, 6525 AJ Nijmegen, The Netherlands

(Received 16 June 2017; accepted 27 July 2017; published online 31 August 2017)

We derive the theory of collision-induced absorption for electronic transitions in the approximation of an isotropic interaction potential. We apply this theory to the spin-forbidden $X^3\Sigma_g^- \rightarrow a^1\Delta_g$ and $X^3\Sigma_g^- \rightarrow b^1\Sigma_g^+$ transitions in O_2–O_2, which are relevant for calibration in atmospheric studies. We consider two mechanisms for breaking the spin symmetry, either by the intermolecular exchange interaction between paramagnetic collision partners or by the intramolecular spin-orbit coupling. The calculations for the exchange-based mechanism employ the diabatic potential energy surfaces and transition dipole moment surfaces reported in Paper I [T. Karman *et al.*, J. Chem. Phys. **147**, 084306 (2017)]. We show that the line shape of the theoretical absorption spectra is insensitive to the large uncertainty in the electronic transition dipole moment surfaces. We also perform calculations using a simple model of the alternative mechanism involving intramolecular spin-orbit coupling, which leads to absorption intensities which are well below the experimental results. The relative intensity of this spin-orbit-based mechanism may impact the relative contribution to the absorption by collisions with diamagnetic collision partners, such as the atmospherically relevant N_2 molecule. We furthermore show that both the line shape and temperature dependence are signatures of the underlying transition mechanism. *Published by AIP Publishing.* [http://dx.doi.org/10.1063/1.4990662]

I. INTRODUCTION

Carbon dioxide is the most abundant greenhouse gas in the Earth's atmosphere, the concentration of which has been increasing throughout the industrial age. This increasing concentration leads to increased surface warming and affects the Earth's climate, making it important to understand and quantify the Earth's carbon cycle by identifying sources and sinks of carbon dioxide.[1] This is attempted by the high-precision measurement of the carbon dioxide concentration using both ground-based and space-borne remote sensing missions, such as the NASA Orbiting Carbon Observatory (OCO-2) satellite.[1] The main factor limiting the accuracy of these retrieval studies is the calibration of the instruments.[2–4]

The OCO-2 satellite instruments are calibrated using the oxygen A-band $X^3\Sigma_g^- \rightarrow b^1\Sigma_g^+$ transition, which is convenient both because the A-band is isolated in the atmospheric spectrum and because the oxygen concentration is known throughout the atmosphere.[2,5–7] The limiting factor remains the accuracy to which the line shape of the oxygen A-band transitions are known. Calibration is sensitive to the region between the saturated magnetic dipole transitions, and hence subtle effects such as collision-induced absorption, line-mixing, and Dicke narrowing are significant. Of these collisional effects, collision-induced absorption has been identified as the largest source of uncertainty in atmospheric retrieval studies.[4]

Measurements determine the total absorption near forbidden transitions in molecular oxygen and subsequently disentangle the different contributions using models of the underlying collisional effects. Therefore, it is important to distinguish the physical origin of the different collisional effects, most notably pressure broadening, shifting, line mixing and collision-induced absorption. Elastic collisions of the absorbing molecule with a perturbing molecule lead to pressure-induced broadening and shifts of the monomer transitions, which follow a Lorentzian line shape. Inelastic collisions give rise to coupling between the different rotational lines known as line mixing, which results in a deviation from the Lorentzian line shape. Collision-induced absorption is a different process in which a photon is absorbed *during* the collision of two molecules. Hence, the molecular collision becomes a source of absorption, rather than a mere perturbation of the absorption process which redistributes spectral intensity.[8]

The oxygen A-band transition, $X^3\Sigma_g^- \rightarrow b^1\Sigma_g^+$, at $\omega = 13\,122\ \mathrm{cm}^{-1}$ is electric dipole forbidden, as the electron spin is not conserved, $S = 1 \nleftrightarrow 0$, and parity is conserved, $g \nleftrightarrow g$. However, first-order spin-orbit coupling mixes the $\Omega = 0$ component of the $X^3\Sigma_g^-$ ground state and the $b^1\Sigma_g^+$ excited state, and hence the transition gains intensity as a magnetic dipole transition.[9] The line shape of this spin-orbit-mediated magnetic-dipole transition is influenced by line mixing, due to inelastic scattering with atmospherically relevant collision partners, most dominantly N_2 and O_2. Spin and inversion symmetry may also be broken by the exchange interaction with a colliding paramagnetic molecule, leading to electric-dipole-allowed collision-induced absorption.[10,11] In the Earth's atmosphere, the most abundant paramagnetic molecule is O_2 itself, and

a)Electronic mail: gerritg@theochem.ru.nl

the oxygen A-band collision-induced absorption should be dominated by O_2–O_2 collisions.

The oxygen $X^3\Sigma_g^- \rightarrow a^1\Delta_g$ transition at $\omega = 7883\ \mathrm{cm}^{-1}$ is also electric-dipole forbidden by both spin and spatial selection rules. This transition also gains some intensity as a magnetic dipole transition due to spin-orbit coupling but is much weaker than the A-band. Rather than direct coupling between the states involved, the mechanism here involves excited states of $^1\Pi_g$ and $^3\Pi_g$ symmetry as intermediate states.[10,12] Electric quadrupole transitions have also been observed for this transition,[13] due to spin-orbit coupling between the $\Omega = 0$ ground state and the $b^1\Sigma_g^+$ excited state, which allows for intensity borrowing from the $b^1\Sigma_g^+ \rightarrow a^1\Delta_g$ Noxon transition. Collision-induced absorption in this band may gain intensity by the same mechanism as discussed above: The exchange coupling with a second paramagnetic molecule leads to a non-zero electric transition dipole moment.[10,11] This again means that collision-induced absorption in this band should be dominated by O_2–O_2 collisions under atmospherically relevant conditions.

On the theoretical side, there has been progress in describing line mixing of the oxygen A-band. Tran *et al.* performed calculations of the relaxation matrix in the energy-corrected sudden approximation for O_2–O_2 and O_2–N_2[14] and Grimminck *et al.* calculated line-mixing using full coupled-channels calculations for the O_2–He system.[15] In fact, the theoretical relaxation matrices computed by Tran *et al.*[14] are used in the most recent and detailed analysis of the oxygen A-band for remote sensing.[16] For collision-induced absorption, the theory for rotation-translation spectra as well as vibrational transitions has been developed, but to our knowledge this theory has not before been extended to electronic transitions. Therefore, a theoretical treatment of collision-induced absorption for electronic transitions in oxygen is timely and is the subject of the present paper.

On the experimental side, the atmospheric application to satellite calibration has motivated numerous high quality and high resolution studies of the oxygen A-band, not all of which included collision-induced absorption. The first measurement of collision-induced absorption in the oxygen A-band was performed by Tabisz *et al.*[17] More recently, the A-band spectrum was revisited by Tran *et al.*,[14] Spiering *et al.*,[18] and Long *et al.*[19] Recently, spectra from a number of different sources were analyzed simultaneously in a multi-spectrum fitting approach by Drouin *et al.*[16] This last study was aimed specifically at reducing the systematic differences between spectra recorded using different instruments for oxygen A-band retrieval. All of the above authors report collision-induced absorption spectra with intensities that are comparable but not in agreement within the error bars and with significant differences in the line shape. One source of this discrepancy may be the analysis through which the collision-induced absorption spectrum is obtained from the total absorption by subtracting the magnetic dipole lines including line mixing, usually starting from the relaxation matrix reported by Tran *et al.*[14] The work of Spiering *et al.*[18] employed the adjustable branch coupling line-mixing model in Ref. 20.

In spite of the efforts invested in the determination of the oxygen A-band collision-induced absorption, some open issues remain. As noted above, there are still some discrepancies between the experimentally determined line shapes and intensities. A second question is the nature of the mechanism leading to the breaking of spin symmetry and collision-induced absorption: Is it the exchange interaction with a second paramagnetic molecule or is it the monomer spin-orbit interaction? This is a fundamental question, but at a practical level, its answer determines whether one should expect collision-induced absorption due to O_2–N_2 collisions to be negligible[15] or comparable[14] to O_2–O_2. Another aspect which may affect atmospheric applications is the temperature dependence of the collision-induced absorption spectrum. In previous experimental studies, only a weak temperature dependence is found between 200 K and 300 K.[14,21] However, one could expect a steep energy dependence for the exchange-driven mechanism for collision-induced absorption,[22] due to the exponentially short-ranged transition dipole moment.

In this paper, we theoretically study collision-induced absorption for spin-forbidden electronic transitions. To this end, we derive the theory of collision-induced absorption for electronic excitations in the isotropic interaction approximation and apply the theory to the $X^3\Sigma_g^- \rightarrow a^1\Delta_g$ and $X^3\Sigma_g^- \rightarrow b^1\Sigma_g^+$ transitions in O_2–O_2. We employ the *ab initio* diabatic potential energy and transition dipole moment surfaces reported in Paper I.[23] We sample the effect of the large uncertainty in the transition dipole moment by computing absorption spectra using surfaces computed at two levels of theory and focus on conclusions that can be drawn independently of the precise dipole moment function. In this way, we hope to contribute to the understanding of collision-induced absorption for electronic transitions of molecular oxygen relevant for atmospheric retrieval studies, the theoretical treatment of which thus far has been lacking.

II. ISOTROPIC-INTERACTION LINE-SHAPE THEORY

In this section, we derive the theory of collision-induced absorption for electronic transitions in collisions of diatomic molecules in arbitrary electronic states. We employ the isotropic interaction approximation throughout. For the rotation-translation collision-induced absorption spectra of first-row diatomics, such as N_2–N_2,[24] the isotropic interaction approximation is expected to be accurate to about 20% at liquid nitrogen temperature and increasingly more accurate for higher temperatures. For electronic excitations, studied in this work, the effects of anisotropy may be more pronounced, but we expect the results of our line-shape calculations to be qualitatively correct. We further neglect the effects of exchange symmetry between identical O_2 moieties, which should be an excellent approximation.[25]

In first-order perturbation theory, the absorption coefficient at frequency ω is given by

$$\alpha(\omega, T) = \frac{2\pi^2}{3\hbar c} n^2 \omega \left[1 - \exp\left(-\frac{\hbar\omega}{k_B T}\right)\right] V g(\omega, T) \qquad (1)$$

with the spectral density

$$g(\omega, T) = \sum_i \sum_f P^{(i)}(T) |\langle i|\hat{\boldsymbol{\mu}}|f\rangle|^2 \delta(\omega_f - \omega_i - \omega). \qquad (2)$$

Here, n, V, and T are the number density, volume, and temperature of the gas, respectively, c is the speed of light, $\hbar$ is the reduced Planck constant, and $\hat{\boldsymbol{\mu}}$ represents the dipole operator. The symbol $\sum\!\!\!\!\!\!\int$ denotes summation over discrete quantum states, i.e., rotation, vibration, and electronic wavefunctions, and integration over the continuum of translational states. The states $|i\rangle$ and $|f\rangle$ represent the initial and final states, with energies $\hbar\omega_i$ and $\hbar\omega_f$, and $P^{(i)}(T)$ is the Boltzmann factor for the initial state.

In what follows, we derive the working equations to calculate the spectral density, Eq. (2), for electronic transitions. Section II A describes the approach for the exchange-based mechanism, which evaluates Eq. (2) using the transition dipole moment surfaces of Paper I.[23] In Sec. II B, we consider the modifications necessary to describe the spin-orbit-based transition mechanism. Finally, we give computational details in Sec. II C. This applies to calculations for both transition mechanisms.

A. Exchange-based mechanism

We begin this section by describing the monomer wavefunctions, labeled with the vibrational quantum number, v_X, electronic state, ψ_X, rotational angular momentum, N_X, and space-fixed projection, m_X. Explicitly, we use the uncoupled ro-vibronic wavefunctions given by

$$\langle \boldsymbol{r}_X | v_X \psi_X N_X m_X \rangle = \langle r_X | v_X \rangle \sqrt{\frac{(N_X)}{4\pi}} D^{(N_X)*}_{m_X,\Lambda_X}(\boldsymbol{r}_X) \left[\hat{\mathcal{R}}(\boldsymbol{r}_X) |\psi_X\rangle \right] |S_X m_{S_X}\rangle , \quad (3)$$

where $\langle r_X | v_X \rangle$ is a vibrational wavefunction and the rotational wavefunction $D^{(N_X)*}_{m_X,\Lambda_X}(\boldsymbol{r}_X)$ is a complex-conjugate Wigner D-matrix element depending on the polar angles of the molecular axis, $\boldsymbol{r}_X$, that is, the zyz Euler angles $(\phi_X, \theta_X, 0)$. We use the short-hand notation $(N) = 2N + 1$. The notation of the spin state is implicit in the left-hand side of Eq. (3), as explained in the following paragraph. The quantity in square brackets is the diabatic electronic wavefunction introduced in Paper I,[23] obtained by rotating the spatial part of a fixed monomer electronic state, $|\psi_X\rangle$, along with the nuclei using the rotation operator

$$\hat{\mathcal{R}}(\boldsymbol{r}_X) = \exp(-i\phi_X \hat{L}_z) \exp(-i\theta_X \hat{L}_y), \quad (4)$$

where θ_X, ϕ_X are the polar angles of $\boldsymbol{r}_X$ and $\hat{\boldsymbol{L}}$ is the electronic orbital angular momentum operator.

In the notation on the left-hand side of Eq. (3), the space-fixed spin state $|S_X m_{S_X}\rangle$ is implicit. The reason for this is that we consider the monomer spins to be coupled to a total triplet,

$$\begin{aligned}\langle \boldsymbol{r}_A | v_A \psi_A N_A m_A \rangle \langle \boldsymbol{r}_B | v_B \psi_B N_B m_B \rangle &= \sum_{m_{S_A}, m_{S_B}} \left\{ \langle r_A | v_A \rangle \sqrt{\frac{(N_A)}{4\pi}} D^{(N_A)*}_{m_A,\Lambda_A}(\boldsymbol{r}_A) \left[\hat{\mathcal{R}}(\boldsymbol{r}_A) |\psi_A\rangle \right] |S_A m_{S_A}\rangle \right\} \\ &\times \left\{ \langle r_B | v_B \rangle \sqrt{\frac{(N_B)}{4\pi}} D^{(N_B)*}_{m_B,\Lambda_B}(\boldsymbol{r}_B) \left[\hat{\mathcal{R}}(\boldsymbol{r}_B) |\psi_B\rangle \right] |S_B m_{S_B}\rangle \right\} \\ &\times \langle S_A m_{S_A} S_B m_{S_B} | 1 M_S \rangle, \end{aligned} \quad (5)$$

where the symbol $\langle S_A m_{S_A} S_B m_{S_B} | S M_S \rangle$ is a Clebsch-Gordan coefficient that serves to couple the monomer spin-states to an overall spin-triplet. Only the triplet total-spin-states of the complex have non-zero transition dipole moments induced by the intermolecular exchange interaction.[23] Therefore, only the contributing collisions take place on the triplet ground-state potential energy surface, but otherwise the electron spin plays no role in the dynamics.

We note that the treatment above requires neglect of small spin-dependent terms in the monomer Hamiltonian, i.e., spin-spin and spin-rotation coupling, which would otherwise couple the spin and rotational angular momenta. For further brevity of notation, we introduce the short-hand $|\boldsymbol{\psi}_X m_X\rangle = |v_X \psi_X N_X m_X\rangle$.

In the isotropic interaction approximation used throughout this paper, we neglect the dependence of the potential on the orientations of the interacting molecules. This orientation-independent potential is readily obtained by removing all terms in the spherical expansion of the potentials except for terms with $L_A = L_B = L = 0$. This means that all off-diagonal diabatic potentials vanish and that the diagonal potentials for states correlating to the same electronic limit are all equal and functions of the intermolecular separation alone.[23]

In this approximation, each partial wave takes the form of a product of the previously defined ro-vibronic states, $|\boldsymbol{\psi}_X m_X\rangle$, for each monomer $X = A, B$, a spherical harmonic describing the end-over-end rotation, $|\ell m_\ell\rangle$, and a radial wavefunction

$$\begin{aligned} |i\rangle, |f\rangle \rightarrow |\boldsymbol{\psi}_A m_A\rangle |\boldsymbol{\psi}_B m_B\rangle |\ell m_\ell\rangle |\boldsymbol{\psi}_A \boldsymbol{\psi}_B \ell E_{\rm col}\rangle , \\ \langle R | \boldsymbol{\psi}_A \boldsymbol{\psi}_B \ell E_{\rm col}\rangle = \frac{1}{R} U^{v_A,\psi_A,v_B,\psi_B}_{E,\ell}(R). \end{aligned} \quad (6)$$

The radial wavefunctions are solutions to

$$\left\{ \frac{d^2}{dR^2} - 2\mu \left[\frac{\ell(\ell+1)}{2\mu R^2} + V^{v_A,\psi_A,v_B,\psi_B}_{0,0,0}(R) - E_{\rm col} \right] \right\} \times U^{v_A,\psi_A,v_B,\psi_B}_{E_{\rm col},\ell}(R) = 0, \quad (7)$$

subject to boundary conditions for small R,

$$U^{v_A,\psi_A,v_B,\psi_B}_{E_{\rm col},\ell}(0) = 0, \quad (8)$$

and for asymptotically large R,

$$U^{v_A,\psi_A,v_B,\psi_B}_{E_{\rm col},\ell}(R) \simeq \frac{R}{\hbar} \sqrt{\frac{\mu k}{2\pi}} \left[h^{(2)}_\ell(kR) + S^{v_A,\psi_A,v_B,\psi_B}_\ell(k) h^{(1)}_\ell(kR) \right]. \quad (9)$$

In the above, $V^{v_A,\psi_A,v_B,\psi_B}_{0,0,0}(R)$ is the vibrationally averaged isotropic potential for the given vibronic state, μ is the reduced mass, E_{col} is the collision energy, $k = \sqrt{2\mu E_{\rm col}}$ is the wave number, ℓ is the partial wave quantum number, and $h^{(1)}_\ell$ and $h^{(2)}_\ell$ denote spherical Hankel functions of the first and second kinds, respectively.[26] The advantage of the isotropic interaction approximation is that the radial coordinate is separated from the vibrational, rotational, and electronic degrees of freedom, such that only the radial wavefunction has to be determined numerically, in a computationally inexpensive single channel scattering calculation. For further brevity of notation, we drop the explicit vibronic state dependence of the radial wavefunctions, $|\ell E_{\rm col}\rangle = |\boldsymbol{\psi}_A \boldsymbol{\psi}_B \ell E_{\rm col}\rangle$.

In order to evaluate the spectral density, $g(\omega, T)$, we need to calculate matrix elements of the dipole operator of the form

$$\langle \boldsymbol{\psi}_A m_A \boldsymbol{\psi}_B m_B \ell m_\ell E_{\rm col} | \hat{\mu}_\kappa | \boldsymbol{\psi}'_A m'_A \boldsymbol{\psi}'_B m'_B \ell' m'_\ell E'_{\rm col} \rangle. \quad (10)$$

The initial and final state wave numbers are indicated as unprimed and primed, respectively. The final-state collision energy is determined by integration over the delta-function in Eq. (2) and is given by

$$\begin{aligned} E'_{\rm col} &= E_{\rm col} + \hbar\omega + E_{v_A,\psi_A} - E_{v'_A,\psi'_A} + E_{v_B,\psi_B} - E_{v'_B,\psi'_B} \\ &= E_{\rm col} + \hbar\Delta\omega, \end{aligned} \quad (11)$$

with $\Delta\omega$ the detuning from the vibration-electronic transition. The operator $\hat{\mu}_\kappa$ denotes the $\kappa = 0, \pm 1$ spherical component of the dipole operator, which is related to the usual Cartesian components by $\mu_0 = \mu_z$, $\mu_{\pm 1} = \mp(\mu_x \pm i\mu_y)/\sqrt{2}$. Matrix elements of the dipole operator between electronic states yield the exchange-induced transition dipole moment surface of Paper I[23] and are given by the expansion

$$\begin{aligned} &\langle \psi_{A,\Lambda_A} \psi_{B,\Lambda_B} | \hat{\mu}_\nu | \psi'_{A,\Lambda'_A} \psi'_{B,\Lambda'_B} \rangle^{(\boldsymbol{r}_A, \boldsymbol{r}_B, \boldsymbol{R})} \\ &\quad = \sum_{L_A,L_B,\lambda,L} \mathcal{D}^{\psi_{A,\Lambda_A},\psi_{B,\Lambda_B},\psi'_{A,\Lambda'_A},\psi'_{B,\Lambda'_B}}_{L_A,L_B,\lambda,L}(R) \\ &\quad \times \sum_{M_A,M_B,\mu,M} \langle L_A M_A L_B M_B | \lambda\mu \rangle \langle \lambda\mu LM | 1\nu \rangle \\ &\quad \times D^{(L_A)*}_{M_A,\Lambda_A-\Lambda'_A}(\phi_A, \theta_A, \psi_A) D^{(L_B)*}_{M_B,\Lambda_B-\Lambda'_B} \\ &\quad \times (\phi_B, \theta_B, \psi_B) C_{L,M}(\Theta, \Phi). \end{aligned} \quad (12)$$

The spectral density, Eq. (2), contains squared matrix elements of the dipole operator, summed over all monomer states. In the isotropic interaction approximation, the sum over all projection quantum numbers can be performed analytically. This requires straightforward angular momentum algebra, involving only the orthogonality of Clebsch-Gordan coefficients, but produces rather lengthy equations which are displayed in Appendix A. The result is given by

$$\begin{aligned} &\sum_{m_A,m_B,m_\ell,m'_A,m'_B,m'_\ell} \left| \langle \boldsymbol{\psi}_A m_A \boldsymbol{\psi}_B m_B \ell m_\ell E_{\rm col} | \hat{\mu}_\kappa | \boldsymbol{\psi}'_A m'_A \boldsymbol{\psi}'_B m'_B \ell' m'_\ell E'_{\rm col} \rangle \right|^2 \\ &\quad = |\langle v''_A | v'_A \rangle|^2 |\langle v''_B | v'_B \rangle|^2 \frac{(N'_A)(N'_B)(\ell')}{(L_A)(L_B)(L)} \sum_{L_A,L_B,\lambda,L} \langle N'_A, \Lambda'_A, L_A, \Lambda_A - \Lambda'_A | N_A \Lambda_A \rangle^2 \\ &\quad \times \langle N'_B, \Lambda'_B, L_B, \Lambda_B - \Lambda'_B | N_B \Lambda_B \rangle^2 \langle \ell' 0 L 0 | \ell 0 \rangle^2 \left| \langle \ell E_{\rm col} | \mathcal{D}^{\psi_A,\psi_B,\psi'_A,\psi'_B}_{L_A,L_B,\lambda,L}(R) | \ell' E'_{\rm col} \rangle \right|^2. \end{aligned} \quad (13)$$

In obtaining this result, we have neglected the vibrational dependence of the potential energy and transition dipole moment surfaces, such that the vibrational dependence is contained completely in the product of Franck-Condon factors, $|\langle v''_A | v'_A \rangle|^2 |\langle v''_B | v'_B \rangle|^2$.

We assume all molecules to be in the ground vibronic state initially, such that the Boltzmann factor in Eq. (2) is given by

$$\begin{aligned} P^{(i)}(T) &= \frac{1}{3} P_{\rm trans} P_{N_A} P_{N_B}, \\ P_{\rm trans} &= \frac{\lambda_0^3}{V} \exp\left(-\frac{E_{\rm col}}{k_B T}\right), \\ \lambda_0 &= \hbar \sqrt{\frac{2\pi}{\mu k T}}, \\ P_{N_X} &= \frac{g_{N_X}}{Z_{\rm rot}} \exp\left(-\frac{E_{{\rm rot},N_X}}{k_B T}\right), \\ Z_{\rm rot} &= \textstyle\sum_{N_X} (2N_X + 1) g_{N_X} \exp\left(-\frac{E_{{\rm rot},N_X}}{k_B T}\right). \end{aligned} \quad (14)$$

The factor 1/3 in the Boltzmann factor arises because only collisions with triplet total spin contribute to the absorption for the transitions considered in this work: The interaction of two triplet ground-state molecules gives rise to one singlet, three triplet, and five quintet spin-substates, thus 3/9 = 1/3 of the spin substates contributes to collision-induced absorption. For ground state oxygen, the statistical weights are $g_{NX} = 0$ if N_X is even and $g_{NX} = 1$ if N_X is odd. The spectral density for absorption due to a transition $\psi_A(v''_A)$, $\psi_B(v''_B) \rightarrow \psi'_A(v'_A)$, $\psi'_B(v'_B)$ at detuning $\Delta\omega$ is given by

$$\begin{aligned} Vg(\Delta\omega) &= \frac{1}{3} |\langle v''_A | v'_A \rangle|^2 |\langle v''_B | v'_B \rangle|^2 \\ &\quad \times \sum_{L_A,L_B,\lambda,L} \sum_{N_A,N_B,N'_A,N'_B} P_{N_A} P_{N_B} \frac{(1)(N_A)(N'_A)(N_B)(N'_B)}{(L_A)(L_B)(L)} \\ &\quad \times \begin{pmatrix} N_A & L_A & N'_A \\ -\Lambda_A & \Lambda_A - \Lambda'_A & \Lambda'_A \end{pmatrix}^2 \begin{pmatrix} N_B & L_B & N'_B \\ -\Lambda_B & \Lambda_B - \Lambda'_B & \Lambda'_B \end{pmatrix}^2 \\ &\quad \times VG^{\psi_A,\psi_B,\psi'_A,\psi'_B}_{L_A,L_B,\lambda,L}(\Delta\omega - \omega^{(N_A,N_B,N'_A,N'_B)}_{\rm rot}), \end{aligned} \quad (15)$$

where the symbols in round brackets are Wigner 3-*jm* symbols, and

$$\begin{aligned} VG^{\psi_A,\psi_B,\psi'_A,\psi'_B}_{L_A,L_B,\lambda,L}(\omega) &= \hbar\lambda_0^3 \sum_{\ell,\ell'} (\ell)(\ell') \begin{pmatrix} \ell & L & \ell' \\ 0 & 0 & 0 \end{pmatrix}^2 \\ &\quad \times \int_0^\infty dE_{\rm col} \exp\left(-\frac{E_{\rm col}}{k_B T}\right) \\ &\quad \times |\langle \ell E_{\rm col} | \mathcal{D}^{\psi_A,\psi_B,\psi'_A,\psi'_B}_{L_A,L_B,\lambda,L}(R) | \ell' E_{\rm col} + \hbar\omega \rangle|^2. \end{aligned} \quad (16)$$

Thus, the spectral density can be thought of as the incoherent superposition of a translational profile, $VG^{\psi_A,\psi_B,\psi'_A,\psi'_B}_{L_A,L_B,\lambda,L}(\omega)$, centered at each ro-vibronic transition at detuning

$\Delta\omega - \omega_{\rm rot}^{(N_A,N_B,N'_A,N'_B)}$, where $\hbar\omega_{\rm rot}^{(N_A,N_B,N'_A,N'_B)} = E'_{\rm rot} - E_{\rm rot}$. We stress that the present derivation applies to the exchange-driven transition mechanism, where the intermolecular exchange induces a transition dipole moment between the total spin-triplet states of the complex. In Eq. (16), the details of the exchange-induced transition dipole moment are completely contained in the angular expansion coefficients, $\mathcal{D}^{\psi_A,\psi_B,\psi'_A,\psi'_B}_{L_A,L_B,\lambda,L}(R)$.

We consider single transitions from the vibronic ground state, $X^3\Sigma_g^-(v''=0)$, to final states $a^1\Delta_g(v')$ and $b^1\Sigma_g^+(v')$; however, either molecule A or B could undergo the transition, and for the $a^1\Delta_g$, the transition could be to either component. These transitions contribute to the same frequency region and can be summed using the symmetry properties of the dipole-moment expansion coefficients. This yields for the different bands

$$
\begin{aligned}
Vg^{X^3\Sigma_g^-(v''=0)\to a^1\Delta_g(v')}(\Delta\omega) &= \frac{4}{3}|\langle 0|v'\rangle|^2 \sum_{L_A,L_B,\lambda,L}\sum_{N_A,N_B,N'_A,N'_B} P_{N_A}P_{N_B}\frac{(1)(N_A)(N'_A)(N_B)(N'_B)}{(L_A)(L_B)(L)} \\
&\quad\times\begin{pmatrix} N_A & L_A & N'_A \\ 0 & -2 & 2\end{pmatrix}^2\begin{pmatrix} N_B & L_B & N'_B \\ 0 & 0 & 0\end{pmatrix}^2 VG^{X^3\Sigma_g^-,X^3\Sigma_g^-,a^1\Delta_{+2},X^3\Sigma_g^-}_{L_A,L_B,\lambda,L}(\Delta\omega-\omega_{\rm rot}^{(N_A,N_B,N'_A,N'_B)}), \\
Vg^{X^3\Sigma_g^-(v''=0)\to b^1\Sigma_g^+(v')}(\Delta\omega) &= \frac{2}{3}|\langle 0|v'\rangle|^2 \sum_{L_A,L_B,\lambda,L}\sum_{N_A,N_B,N'_A,N'_B} P_{N_A}P_{N_B}\frac{(1)(N_A)(N'_A)(N_B)(N'_B)}{(L_A)(L_B)(L)} \\
&\quad\times\begin{pmatrix} N_A & L_A & N'_A \\ 0 & 0 & 0\end{pmatrix}^2\begin{pmatrix} N_B & L_B & N'_B \\ 0 & 0 & 0\end{pmatrix}^2 VG^{X^3\Sigma_g^-,X^3\Sigma_g^-,b^1\Sigma_g^+,X^3\Sigma_g^-}_{L_A,L_B,\lambda,L}(\Delta\omega-\omega_{\rm rot}^{(N_A,N_B,N'_A,N'_B)}),
\end{aligned}
\tag{17}
$$

and we assume that the different vibronic bands do not overlap.

B. Spin-orbit mechanism

In this section, we derive a model for the line shape of collision-induced absorption through a spin-orbit-based mechanism, i.e., where the spin-selection rules are lifted by intramolecular spin-orbit coupling rather than by the intermolecular exchange interaction. The spin-orbit interaction directly couples the $\Omega=\Sigma=0$ component of the $X^3\Sigma_g^-$ ground state and the $b^1\Sigma_g^+$ excited state, where Ω and Σ are the body-fixed projections of the total and spin monomer angular momenta, respectively. This direct coupling is the dominant spin-orbit effect because the $b^1\Sigma_g^+$ excited state is exceptionally low-lying and the coupling is relatively strong. This well-established theory of spin-orbit coupling in the O_2 molecule has been pioneered by Minaev and co-workers.[9,12] The spin-orbit interaction mixes the two states

$$
\begin{aligned}
|\Psi_{X,0}\rangle &= \left|X^3\Sigma_g^-\right\rangle + C_{\rm SO}\left|b^1\Sigma_g^+\right\rangle, \\
|\Psi_b\rangle &= \left|b^1\Sigma_g^+\right\rangle - C^*_{\rm SO}\left|X^3\Sigma_g^-\right\rangle,
\end{aligned}
\tag{18}
$$

where the mixing constant can be evaluated using first-order perturbation theory[9]

$$
C_{\rm SO} = \frac{\langle b^1\Sigma_g^+|\hat{H}_{\rm SO}|X^3\Sigma_g^-\rangle}{E_X - E_b} = 0.0134i. \tag{19}
$$

The mixing between the triplet ground state and singlet excited state breaks the spin symmetry, yielding for the spin-allowed electric dipole moments,

$$
\langle a^1\Delta_g|\hat{\mu}_\nu|\Psi_{X,0}\rangle = C_{\rm SO}\langle a^1\Delta_g|\hat{\mu}_\nu|b^1\Sigma_g^+\rangle, \tag{20a}
$$

$$
\langle\Psi_b|\hat{\mu}_\nu|\Psi_{X,0}\rangle = C_{\rm SO}\left[\langle b^1\Sigma_g^+|\hat{\mu}_\nu|b^1\Sigma_g^+\rangle - \langle X^3\Sigma_g^-|\hat{\mu}_\nu|X^3\Sigma_g^-\rangle\right]. \tag{20b}
$$

This electric transition dipole moment still vanishes in the free O_2 monomer due to inversion symmetry but may deviate from zero if the inversion symmetry is broken by interaction with a second molecule.

We note that the spin-orbit mixing described above also gives rise to magnetic dipole and electric quadrupole transitions. These transitions are not parity forbidden and hence lead to narrow monomer absorption lines which are not considered in the present work.

If the collision with a second molecule breaks the inversion symmetry, all terms on the right-hand sides of Eqs. (20a) and (20b) may differ from zero. For the $X^3\Sigma_g^- \to a^1\Delta_g$ transition, Eq. (20a), intensity is borrowed from the collision-induced electric dipole for the $b^1\Sigma_g^+ \to a^1\Delta_g$ Noxon transition. For the $X^3\Sigma_g^- \to b^1\Sigma_g^+$ transition, Eq. (20b), the electric dipole moment is proportional to the *difference* in dipole moment between the ground and excited states. By analogy with the rotation-translation spectra of the N_2–N_2 system,[24] we assume that these dipole surfaces are dominated by first-order quadrupole-induced terms. That is, we assume that the transition dipole surface is given by a single angular component, $\{L_A, L_B, \lambda, L\} = \{2, 0, 2, 3\}$, with coefficient

$$
\begin{aligned}
\mathcal{D}^{{\rm SO},X^3\Sigma_g^-,\Omega\to\psi}_{2,0,2,3} &= c^{(4),X^3\Sigma_g^-,\Omega\to\psi}_{2,0,2,3}R^{-4} \\
&= \sqrt{35}\langle X^3\Sigma_g^-,\Omega|\Theta_A|\psi\rangle\langle X^3\Sigma_g^-|\alpha_B|X^3\Sigma_g^-\rangle R^{-4},
\end{aligned}
\tag{21}
$$

for a $X^3\Sigma_g^- \to \psi = a^1\Delta_g, b^1\Sigma_g^+$ transition in molecule A.

Explicitly, we use the following molecular parameters in atomic units:

$$\langle X^3\Sigma_g^-|\alpha|X^3\Sigma_g^-\rangle = 10.87,$$
$$\langle X^3\Sigma_g^-,\Omega|\Theta|a^1\Delta_g\rangle = \begin{cases} 0.0134i, \text{ for } \Omega = 0, \\ 0, \qquad \text{for } |\Omega| = 1, \end{cases} \tag{22}$$
$$\langle X^3\Sigma_g^-,\Omega|\Theta|b^1\Sigma_g^+\rangle = \begin{cases} 0.0021i, \text{ for } \Omega = 0, \\ 0.0050i, \text{ for } |\Omega| = 1. \end{cases}$$

The O_2 polarizability is taken from Ref. 27. The $X^3\Sigma_g^- \rightarrow a^1\Delta_g$ quadrupole is obtained from

$$\langle \Psi_{X,0}|\hat{\Theta}|a^1\Delta_g\rangle = C_{\rm SO}^*\langle b^1\Sigma_g^+|\hat{\Theta}|a^1\Delta_g\rangle, \tag{23}$$

ab initio values for the spin-orbit mixing, $C_{\rm SO}$, and the Noxon transition quadrupole moment.[9,28] According to this theory, the $X^3\Sigma_g^- \rightarrow a^1\Delta_g$ transition quadrupole moment is dominated by contributions of the $\Omega = 0$ component of the ground state, in good agreement with experimentally observed quadrupole transitions.[13] The $X^3\Sigma_g^- \rightarrow b^1\Sigma_g^+$ transition quadrupole also has significant contributions from the $\Omega = \pm 1$ components, due to the spin-orbit mixing with much higher lying $^1\Pi_g$ and $^3\Pi_g$ states. These weaker perturbations become relevant for this transition as the $\Omega = 0$ component contributes the difference between the $X^3\Sigma_g^-$ and $b^1\Sigma_g^+$ quadrupole moments, which is much smaller than the strong transition quadrupole moment for the $b^1\Sigma_g^+ \rightarrow a^1\Delta_g$ transition. The quadrupole moment used here has been fit to reproduce the experimental electric quadrupole transitions in the A-band.[29–31]

The calculation of the collision-induced absorption spectrum differs only slightly from the formalism outlined in Sec. II. The first difference is that we now use product of Hund's case (b) wavefunctions,

$$\langle \boldsymbol{r}_A|\boldsymbol{\psi}_A m_A\rangle\langle \boldsymbol{r}_B|\boldsymbol{\psi}_B m_B\rangle = \sqrt{\frac{(N_A)}{4\pi}} D^{(N_A)*}_{m_A,\Lambda_A}(\boldsymbol{r}_A)\left[\hat{\mathcal{R}}(\boldsymbol{r}_A)|\psi_A\rangle\right]|S_A m_{S_A}\rangle \times \sqrt{\frac{(N_B)}{4\pi}} D^{(N_B)*}_{m_B,\Lambda_B}(\boldsymbol{r}_B)\left[\hat{\mathcal{R}}(\boldsymbol{r}_B)|\psi_B\rangle\right]|S_B m_{S_B}\rangle, \tag{24}$$

rather than the implicitly total spin-triplet coupled states of Eq. (5). The coupling of the monomer spins was necessary in the case of the exchange-based mechanism, where only the total spin-triplet states contribute to the absorption. Here, the spin selection rules are lifted by intra-molecular spin-orbit coupling. We assume that the potential also does not depend on the coupling of the monomer spins, such that we can integrate out the "spectator" spin degrees of freedom of the perturbing molecule, monomer B. The second difference is that the transition dipole moment is explicitly dependent on the $\Omega = \Sigma$ quantum number of the ground state. In order to calculate matrix elements of the dipole operator, we therefore express the monomer A wavefunction in Hund's case (a) representation,

$$\sqrt{\frac{(N_A)}{4\pi}} D^{(N_A)*}_{m_{N_A},0}(\boldsymbol{r}_A)|S_A m_{S_A}\rangle = \sum_{j_A,m_A,\Sigma_A} \sqrt{\frac{(j_A)}{4\pi}} D^{(j_A)*}_{m_A,\Sigma_A}(\boldsymbol{r}_A)\hat{\mathcal{R}}(\boldsymbol{r}_A)|S_A\Sigma_A\rangle \times \sqrt{\frac{(N_A)}{(j_A)}}\langle N_A m_{N_A} S_A m_{S_A}|j_A m_A\rangle\langle N_A 0 S_A\Sigma_A|j_A\Sigma_A\rangle. \tag{25}$$

With these modifications, the derivation of the spectral density is largely analogous to that in the case of the exchange-based mechanism, and detailed steps are displayed in Appendix B.

The expressions for the spectral density for the spin-orbit-based mechanism are given by

$$Vg^{\mathrm{SO},X^3\Sigma_g^-\rightarrow a^1\Delta_g}(\Delta\omega) = \frac{4}{3}\sum_{L_A,L_B,\lambda,L}\sum_{j_A,N_A,N_B,N'_A,N'_B} P_{N_A}P_{N_B}\frac{(1)(j_A)(N_A)(N'_A)(N_B)(N'_B)}{(L_A)(L_B)(L)} \times \begin{pmatrix} N_A & 1 & j_A \\ 0 & 0 & 0 \end{pmatrix}^2 \begin{pmatrix} j_A & L_A & N'_A \\ 0 & -2 & 2 \end{pmatrix}^2 \begin{pmatrix} N_B & L_B & N'_B \\ 0 & 0 & 0 \end{pmatrix}^2 \times \left| c^{(n),X^3\Sigma_g^-,\Omega\rightarrow a^1\Delta_g}_{L_A,L_B,\lambda,L}\right|^2 VG_L^{R^{-n}}(\Delta\omega - \omega^{(N_A,N_B,N'_A,N'_B)}_{\rm rot}), \tag{26a}$$

$$Vg^{\mathrm{SO},X^3\Sigma_g^-\rightarrow b^1\Sigma_g^+}(\Delta\omega) = \frac{2}{3}\sum_{L_A,L_B,\lambda,L}\sum_{N_A,N_B,N'_A,N'_B} P_{N_A}P_{N_B}\sum_{j_A,\Sigma_A,\Sigma_A}{}' \frac{(1)(j_A)(N_A)(N'_A)(N_B)(N'_B)}{(L_A)(L_B)(L)} \times \begin{pmatrix} N_A & 1 & j_A \\ 0 & \Sigma_A & -\Sigma_A \end{pmatrix}\begin{pmatrix} N_A & 1 & j_A \\ 0 & \Sigma'_A & -\Sigma'_A \end{pmatrix}\begin{pmatrix} j_A & L_A & N'_A \\ -\Sigma_A & \Sigma_A & 0 \end{pmatrix}\begin{pmatrix} j_A & L_A & N'_A \\ -\Sigma'_A & \Sigma'_A & 0 \end{pmatrix} \times \begin{pmatrix} N_B & L_B & N'_B \\ 0 & 0 & 0 \end{pmatrix}^2 c^{(n),X^3\Sigma_g^-,\Sigma_A\rightarrow b^1\Sigma_g^+*}_{L_A,L_B,\lambda,L} c^{(n),X^3\Sigma_g^-,\Sigma'_A\rightarrow b^1\Sigma_g^+}_{L_A,L_B,\lambda,L} \times VG_L^{R^{-n}}(\Delta\omega - \omega^{(N_A,N_B,N'_A,N'_B)}_{\rm rot}). \tag{26b}$$

The long-range coefficients of the dipole moment surface are defined in Eqs. (21) and (22). We have defined the translational profiles for R^{-n} long-ranged dipole moment surfaces as

$$VG_L^{R^{-n}}(\omega) = \hbar\lambda_0^3\sum_{\ell,\ell'}(\ell)(\ell')\begin{pmatrix} \ell & L & \ell' \\ 0 & 0 & 0 \end{pmatrix}^2 \times \int_0^\infty dE_{\rm col}\exp\left(-\frac{E_{\rm col}}{k_B T}\right) \times |\langle \ell E_{\rm col}|R^{-n}|\ell' E_{\rm col} + \hbar\omega\rangle|^2. \tag{27}$$

We note that a factor 1/3 in Eq. (26) is due to the partition sum over the spin-projection quantum number of the absorbing molecule, m_{S_A}, rather than the statistical factor for total spin triplet coupling, which results also in a factor 1/3 in Eq. (17) for the exchange interaction based mechanism.

C. Computational details

Single channel scattering calculations were performed using the Numerov algorithm. Radial wavefunctions were obtained for each partial wave on a discrete grid in the collision energy. This yields the squared radial dipole overlap integrals in Eqs. (16) and (27) on discrete grids in the initial and final energies, E and E', respectively. We obtained these quantities on discrete grids in the initial state energy, E_{col}, and the detuning, $\hbar\omega$, by spline interpolation of the logarithm of the squared integral. The translational profiles were then obtained by performing the integral over the initial state energy using a trapezoidal quadrature rule.[24,25]

Absorption spectra converged with respect to the treatment of the dynamics to better than 1% were obtained using the following parameters. Scattering wavefunctions were propagated on an equidistant radial grid from $R = 4.5\ a_0$ to $30\ a_0$ in steps of $0.017\ a_0$, corresponding to the de Broglie wave length for the highest collision energy considered divided by 15. We included all initial partial waves with $\ell < 150$ and all partial waves of the final state that are coupled to the initial state by the dipole surface of Paper I.[23] The initial state rotational wavefunctions were included for $N_A, N_B < 30$.

The grid in the collision energies has been tailored to exclude unphysical artefacts of the sharp shape resonances supported by the isotropic potentials.[24] The grid essentially corresponds to roughly 75 logarithmically spaced points between 0.1 K and 3000 K. However, we have removed all points that lie on a resonance, i.e., between $E_0 \pm 3\Gamma$, where E_0 is the resonance position and Γ is the resonance width. Points were added above and below each resonance, at $E_0 \pm 3.1\Gamma$, in order to sample only the background contribution. The resonance positions and widths were determined by fitting the energy dependence of the phase shift, $\delta_\ell(E)$, defined by the S-matrix element, $S_\ell = \exp(i2\delta_\ell)$. The phase shift was fit to a constant background and a Breit-Wigner resonant contribution in the vicinity of each grid point,[32] starting from a logarithmically spaced energy grid.

The Franck-Condon factors in Eq. (17) are approximated by unity for the $v'' = 0 \rightarrow v' = 0$ transitions considered here. This is a good approximation for the considered states of O_2 because they correspond to the same electronic configuration and hence have very similar potential curves. Therefore, this should not lead to errors of more than a few percent overall scaling.[33]

III. RESULTS

A. The exchange mechanism for the $X^3\Sigma_g^- \rightarrow b^1\Sigma_g^+$ transition

Figure 1 shows collision-induced absorption spectra for the oxygen A-band $X^3\Sigma_g^- \rightarrow b^1\Sigma_g^+$ transition in O_2–O_2 at room temperature. This figure includes the experimental collision-induced absorption spectra of Refs. 14 and 16, as well as three theoretical spectra. The experiment of Ref. 16 refers to measurements of air, rather than of pure oxygen. Two of the theoretical spectra were obtained using the multireference configuration interaction (MRCI) and complete active space self-consistent field (CASSCF) level transition dipole moment surfaces of Ref. 23, respectively, both using the isotropic potentials from that same reference. The differences between these spectra give an indication of the uncertainty in the spectrum due to the uncertainty in the dipole moment surface. A third theoretical spectrum has been obtained using the same MRCI transition dipole moment, but applying a scaling to the isotropic dispersion coefficient of the potential. The effect of this scaling is indicative of the sensitivity of the spectra with respect to uncertainty in the potential. Large differences between the theoretical predictions and the experimental data occur, although the line shapes of all theoretical spectra and the experimental spectrum of Ref. 14 are similar.

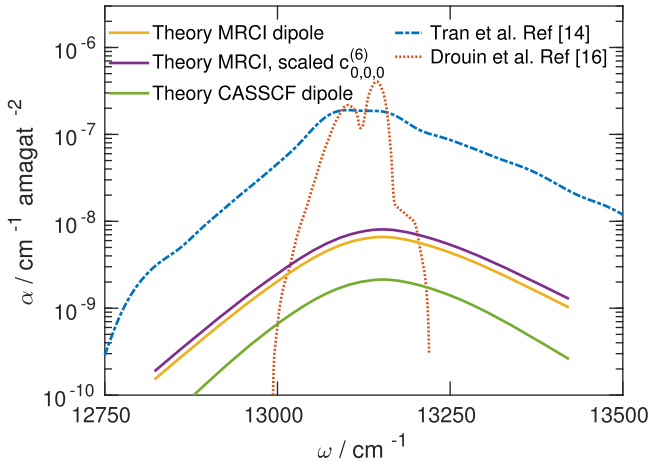

FIG. 1. Collision-induced absorption spectra for the $X^3\Sigma_g^- \rightarrow b^1\Sigma_g^+$ transition in O_2–O_2 at room temperature. The dashed-dotted and dotted lines correspond to the experimentally determined spectra of Refs. 14 and 16, respectively. The solid lines correspond to the theoretical results of the present work using either the MRCI or the CASSCF level dipole surfaces of Paper I,[23] and the isotropic potential energy surfaces of the same reference, with or without scaling applied.

The line shapes can be compared more directly in Fig. 2, which shows the same absorption spectra normalized to the

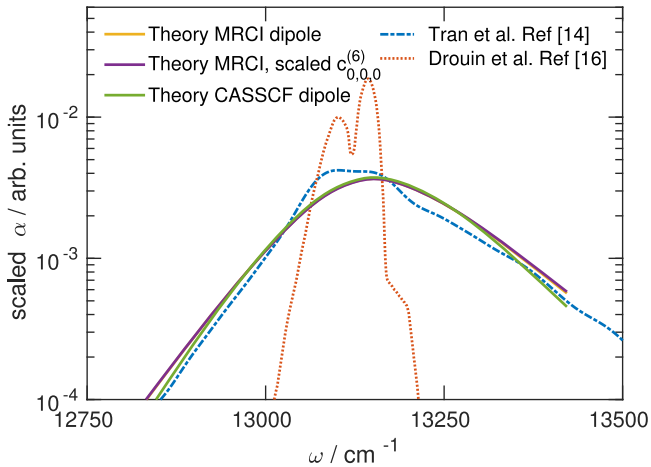

FIG. 2. Collision-induced absorption spectra for the $X^3\Sigma_g^- \rightarrow b^1\Sigma_g^+$ transition in O_2–O_2, scaled in order to normalize the integrated intensity. For a more detailed description of the lines, see Fig. 1 or the legend.

TABLE I. Integrated intensities computed for the various transition dipole moment surfaces and bands studied in this work. Integrated intensities are given in cm^{-2} $amagat^{-2}$ with numbers in parentheses denoting powers of ten.

	T = 300 K	T = 200 K	T = 100 K	T = 78 K
$X^3\Sigma_g^- \rightarrow b^1\Sigma_g^+$				
Exchange, MRCI	1.93 (−6)	1.19 (−6)	6.65 (−7)	5.78 (−7)
Exchange, CASSCF	6.08 (−7)	3.91 (−7)	2.29 (−7)	1.99 (−7)
Spin-orbit	6.23 (−7)	5.99 (−7)	5.80 (−7)	5.73 (−7)
$X^3\Sigma_g^- \rightarrow a^1\Delta_g$				
Exchange, MRCI	2.91 (−5)	2.11 (−5)	1.42 (−5)	1.28 (−5)
Exchange, CASSCF	2.27 (−5)	1.63 (−5)	1.09 (−5)	9.84 (−6)
Spin-orbit	2.35 (−5)	2.25 (−5)	2.14 (−5)	2.10 (−5)

same integrated intensity. The shapes of all theoretical spectra are similar and also agree with the spectrum of Ref. 14. The collision-induced absorption spectrum of Ref. 16 is significantly narrower and more structured. The relatively small spread in the theoretical line shape, in spite of the large uncertainty in the transition dipole surface, can be regarded so as to put restrictions on the possible collision-induced line shapes. Analyzing the experimental oxygen A-band spectra with such line shapes may be a useful avenue of research.

The integrated intensities of the theoretical spectra can be found in Table I. This table also includes the $X^3\Sigma_g^- \rightarrow a^1\Delta_g$ transition, and the spin-orbit-based mechanism for both bands, which are discussed below. We stress that the integrated intensities tabulated here are not necessarily predictive due to the large uncertainty in the transition dipole moment surfaces.[23] Nevertheless, we tabulate the integrated intensities given the dipole moment surfaces of Paper I for reference.[23]

Figure 3 shows the contributions of the most significant angular components of the transition dipole surface. In the isotropic interaction approximation, all angular components contribute incoherently, i.e., additively and without interference terms. Although the dipole moment function is highly anisotropic, the most significant contributions to the absorption spectrum originate from comparatively few and low-rank expansion terms. The corresponding translational profiles can

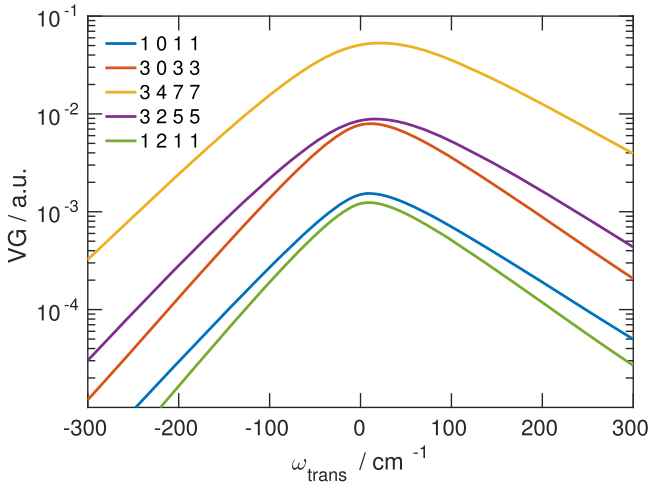

FIG. 4. Translational profiles of the most significant spherical components of the MRCI dipole moment surface.

be seen in Fig. 4. The translational profiles for all angular terms are generally structureless and of comparable width. The typical width is much larger than the rotational splitting and also larger than what is typically observed for rotation-translation spectra.[24] This larger width is attributed to the short range of the exchange-driven electronic transition dipole moment.

The temperature dependence of the theoretical A-band absorption spectrum is shown in Fig. 5. With increasing temperature, the spectrum broadens and gains in intensity. The broadening is also observed for typical rotation-translation spectra and is both due to broadening of the translational profiles and due to the increased thermal population of excited rotational states. The overall increase in intensity does not occur for rotation-translation spectra. We attribute this to the short-ranged nature of the exchange-driven electronic transition dipole moment of the oxygen A-band. With increasing temperature, the colliding molecules approach more closely, leading to a substantial increase in the transition dipole moment. For rotation-translation spectra, the dipole moment is longer ranged and the intensity increase is less substantial. This means that the temperature dependence can be

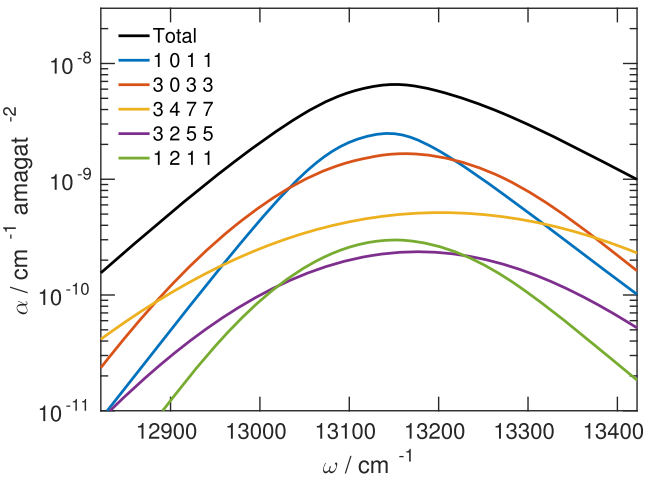

FIG. 3. Contribution of the most significant spherical components of the MRCI dipole moment surface to the collision-induced absorption spectra for the $X^3\Sigma_g^- \rightarrow b^1\Sigma_g^+$ transition in O_2–O_2.

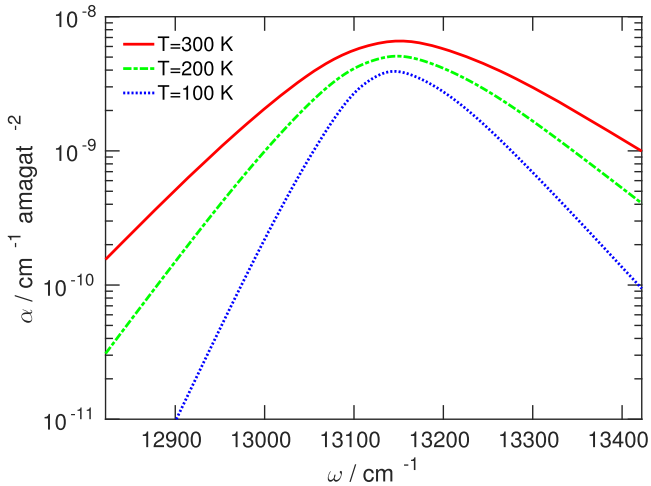

FIG. 5. Temperature dependence of the theoretical collision-induced absorption spectra for the $X^3\Sigma_g^- \rightarrow b^1\Sigma_g^+$ transition in O_2–O_2, using the MRCI dipole moment surface.

used as a probe of the mechanism driving collision-induced transitions.

B. The exchange mechanism for the $X^3\Sigma_g^- \rightarrow a^1\Delta_g$ transition

Collision-induced absorption spectra for the $X^3\Sigma_g^- \rightarrow a^1\Delta_g$ transition in O_2–O_2 at room temperature are shown in Fig. 6. This figure shows the experimental absorption spectrum of Ref. 21, together with two calculations, based on the MRCI and CASSCF level transition dipole moment surfaces of Ref. 23, respectively. The same spectra are shown normalized to unit integrated intensity in Fig. 7. These figures again show that the shape of the theoretical spectra is relatively insensitive to the large uncertainty in the transition dipole moment surface. The theoretical line shape does not exactly match the experimental spectrum, as the experimental line shape is significantly narrower near the line center. The decay of the spectra in the wings seems to match more closely.

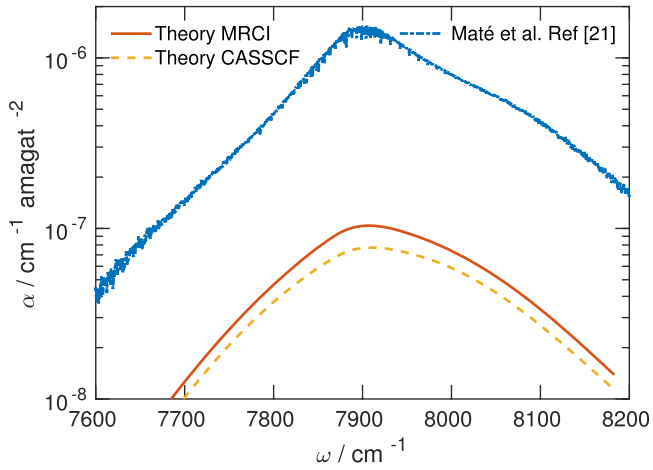

FIG. 6. Collision-induced absorption spectra for the $X^3\Sigma_g^- \rightarrow a^1\Delta_g$ transition in O_2–O_2 at room temperature. The dashed-dotted line corresponds to the experimentally determined spectra of Ref. 21, and the solid line and dashed lines correspond to the theoretical results of the present work using the MRCI or CASSCF level dipole surfaces of Paper I,[23] respectively.

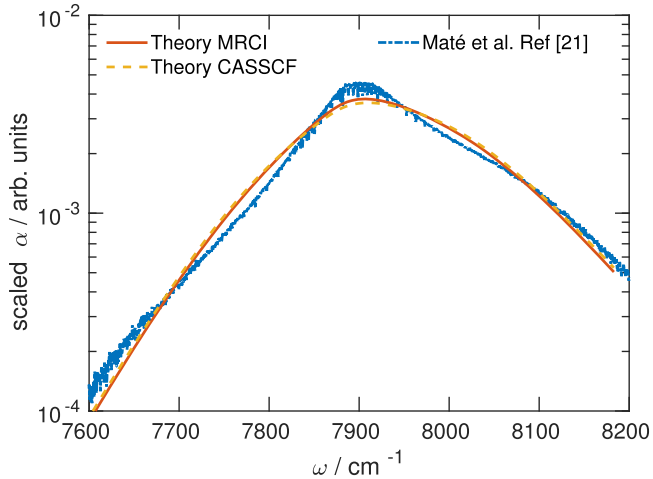

FIG. 7. Collision-induced absorption spectra for the $X^3\Sigma_g^- \rightarrow a^1\Delta_g$ transition in O_2–O_2, scaled in order to normalize the integrated intensity. For a more detailed description of the lines, see Fig. 6 or the legend.

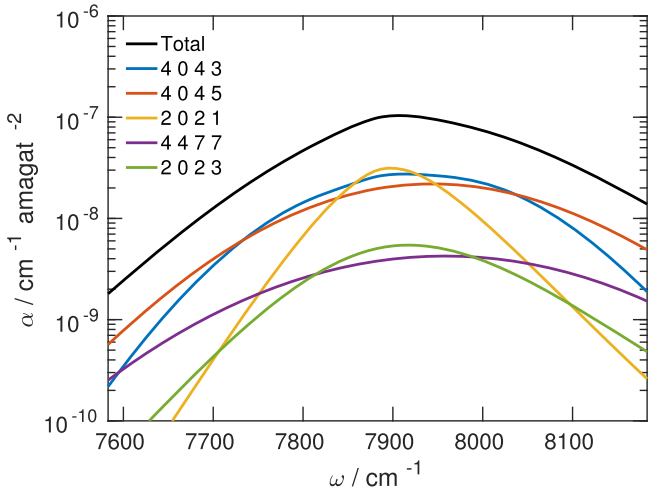

FIG. 8. Contribution of the most significant spherical components of the MRCI dipole moment surface to the collision-induced absorption spectra for the $X^3\Sigma_g^- \rightarrow a^1\Delta_g$ transition in O_2–O_2.

The contributions of different angular expansion terms of the MRCI transition dipole surface are shown in Fig. 8. As for the oxygen A-band, a relatively small number of angular terms contribute significantly, although the transition dipole moment itself is highly anisotropic. This figure suggests that a more narrow line center would have been obtained if the $\{L_A, L_B, \lambda, L\} = \{2, 0, 2, 1\}$ term was more dominant, without affecting the wings of the spectrum.

Figure 9 shows the temperature dependence of the $X^3\Sigma_g^- \rightarrow a^1\Delta_g$ spectrum of O_2–O_2 between $T = 100$ and 300 K. The temperature dependence is similar to what is observed for the oxygen A-band: The absorption spectrum broadens and increases in intensity with increasing temperature.

C. Spin-orbit mechanism for the $X^3\Sigma_g^- \rightarrow b^1\Sigma_g^+$ transition

In this section, we discuss the oxygen A-band spectra computed assuming a simple model for the alternative spin-orbit-based mechanism. This model, derived in Sec. II B,

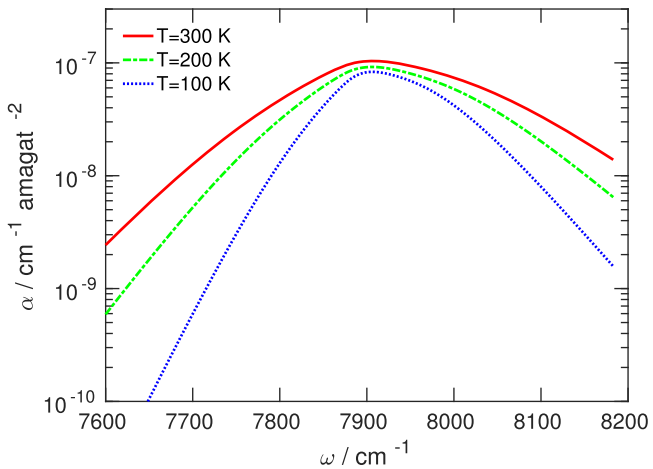

FIG. 9. Temperature dependence of the theoretical collision-induced absorption spectra for the $X^3\Sigma_g^- \rightarrow a^1\Delta_g$ transition in O_2–O_2, using the MRCI dipole moment surface.

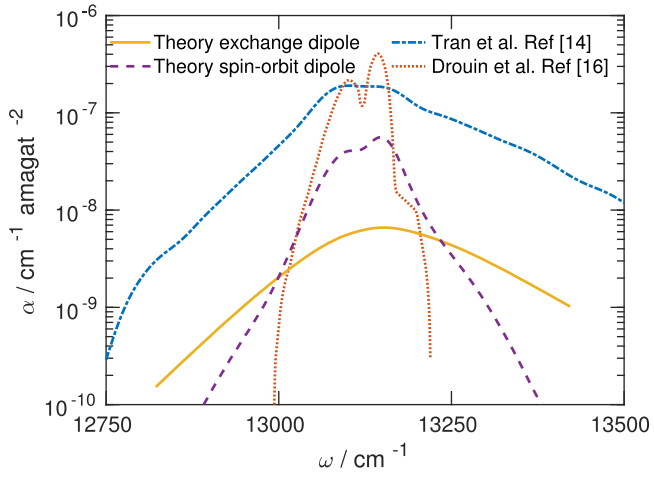

FIG. 10. Collision-induced absorption spectra for the $X^3\Sigma_g^- \rightarrow b^1\Sigma_g^+$ transition in O_2–O_2. The dashed-dotted and dotted lines correspond to the experimentally determined spectra of Refs. 14 and 16, respectively. The solid line corresponds to the theoretical spectrum calculated using the exchange-driven mechanism using the MRCI dipole moment surface. The dashed line corresponds to the theoretical spectrum calculated using the spin-orbit-driven mechanism.

assumes that the spin-symmetry is broken by spin-orbit coupling in the absorbing molecule, the dipole surface is given by its R^{-4} long-range form, and the initial state potential energy does not depend on the exchange interaction, i.e., the spin-splitting of the singlet, triplet, and quintet ground-state potentials is not included.

Figure 10 shows the experimental A-band absorption spectra from Refs. 14 and 16, again the theoretical spectra of the present work using the exchange-driven MRCI transition dipole surface, and the results obtained using the spin-orbit-mediated transition dipole moment. The same spectra, scaled to equal integrated intensity, are shown in Fig. 11 for a more convenient comparison of the line shape. The spin-orbit based mechanism leads to a much narrower profile, albeit still broader than the experimental result in Ref. 16.

The temperature dependence of the theoretical A-band absorption spectrum, assuming the spin-orbit-based mechanism, is shown in Fig. 12. Due to the long-ranged transition

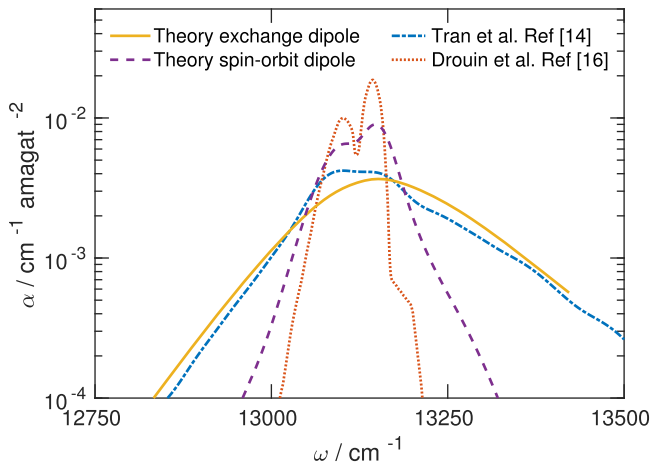

FIG. 11. Collision-induced absorption spectra for the $X^3\Sigma_g^- \rightarrow b^1\Sigma_g^+$ transition in O_2–O_2, scaled in order to normalize the integrated intensity. For a more detailed description of the lines, see Fig. 10 or the legend.

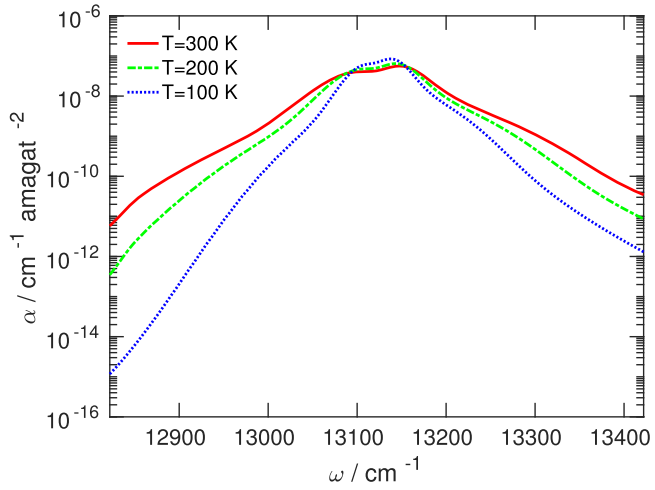

FIG. 12. Temperature dependence of the theoretical collision-induced absorption spectra for the $X^3\Sigma_g^- \rightarrow b^1\Sigma_g^+$ transition, assuming the spin-orbit-mediated mechanism.

dipole moment involved in this mechanism, the temperature dependence is different from what was observed for the exchange-driven mechanism: The absorption spectrum broadens with increasing temperature, but the intensity of the spectrum does not increase. This confirms that the temperature dependence is a probe for the transition mechanism.

We now turn our attention to the absolute intensity of the absorption spectrum in Fig. 10. Thus far, we have not analyzed the intensity of the theoretical spectra in much detail because the intensity is strongly affected by the uncertainty in the exchange-driven transition dipole moment surfaces. For the spin-orbit based mechanism, however, the situation is different because the overall intensity is determined by the $X^3\Sigma_g^- \rightarrow b^1\Sigma_g^+$ transition quadrupole moment and isotropic polarizability. These quantities are known and at least the order of magnitude of the intensity calculated by our simple model should be considered to be predictive. The predicted intensity, however, is well below the experimental results. This suggests that the exchange-driven mechanism is dominant over the mechanism involving the spin-orbit coupling, which is supported further by the closer match in line shape, as discussed above.

It may not be surprising that spin-orbit coupling is not dominant in the collision-induced absorption spectra of O_2–O_2, but it is worth noting that this conclusion may impact the experimental determination of O_2–N_2 collision-induced absorption. In collisions with diamagnetic N_2 molecules, the exchange interaction does not break spin-symmetry, and spin-orbit coupling should determine the O_2–N_2 collision-induced absorption. In a subsequent publication,[34] we study the absorption mechanism in more detail for related vibronic transitions in O_2–O_2 and O_2–N_2, unambiguously identifying the absorption mechanisms.

D. Spin-orbit mechanism for the $X^3\Sigma_g^- \rightarrow a^1\Delta_g$ transition

We have also performed calculations for the $X^3\Sigma_g^- \rightarrow a^1\Delta_g$ transition in the spin-orbit-based mechanism. The absorption spectrum for this mechanism is shown in Fig. 13,

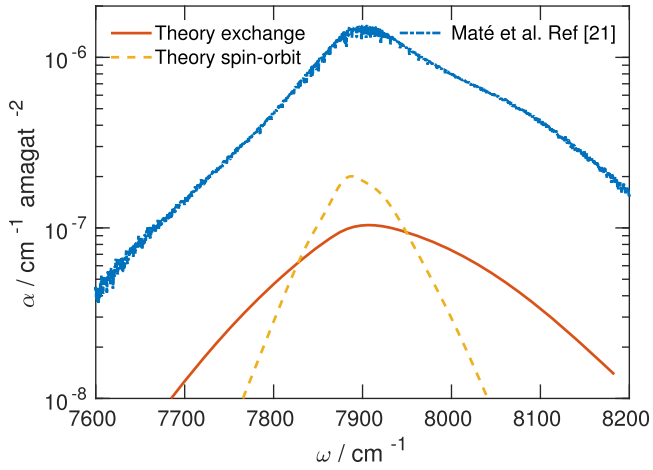

FIG. 13. Collision-induced absorption spectra for the $X^3\Sigma_g^- \rightarrow a^1\Delta_g$ transition in O_2–O_2. The dashed-dotted line corresponds to the experimentally determined spectrum of Ref. 21. The solid line corresponds to the theoretical spectrum calculated using the exchange-driven mechanism using the MRCI dipole moment surface. The dashed line corresponds to the theoretical spectrum calculated using the spin-orbit-driven mechanism.

along with predictions for the exchange-based mechanism discussed before, and the experimental results of Maté *et al.*[21] Again, the obtained line shape for the spin-orbit mechanism is much narrower than both the exchange-based calculation and the experimental result. This can be seen most clearly in Fig. 14, where all spectra are scaled to equal integrated intensity. Also for the $X^3\Sigma_g^- \rightarrow a^1\Delta_g$ transition, the overall intensity of the spin-orbit-based mechanism is significantly below the experimental result, despite the larger transition quadrupole moment for this band. The spin-orbit mechanism could contribute to the narrower line center observed experimentally.

Finally, the temperature dependence of the theoretical spectrum for the spin-orbit mechanism is shown in Fig. 15. The width of the spectrum increases with increasing spectrum, but the integrated intensity is again less temperature dependent.

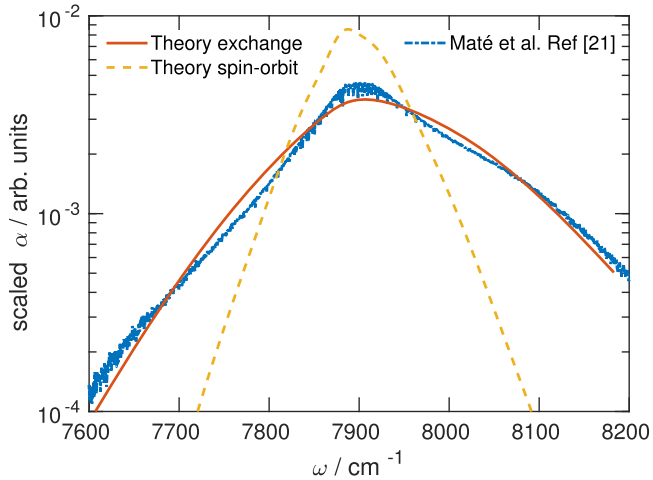

FIG. 14. Collision-induced absorption spectra for the $X^3\Sigma_g^- \rightarrow a^1\Delta_g$ transition in O_2–O_2, scaled in order to normalize the integrated intensity. For a more detailed description of the lines, see Fig. 13 or the legend.

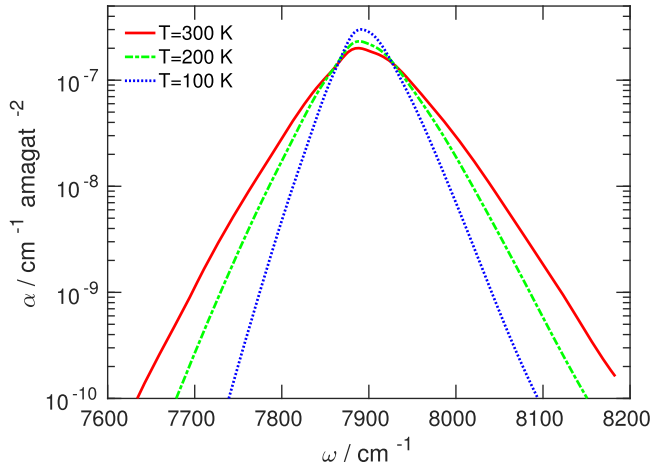

FIG. 15. Temperature dependence of the theoretical collision-induced absorption spectra for the $X^3\Sigma_g^- \rightarrow a^1\Delta_g$ transition, assuming the spin-orbit-mediated mechanism.

IV. CONCLUSIONS

In this paper, we have extended the formalism for computing collision-induced absorption spectra in the isotropic interaction approximation to include electronic excitations. We have applied this theory to the $X^3\Sigma_g^- \rightarrow a^1\Delta_g$ and $X^3\Sigma_g^- \rightarrow b^1\Sigma_g^+$ transitions in O_2–O_2, using the potential energy and transition dipole moment surfaces of Paper I.[23] Collision-induced absorption in the O_2 A-band transition is relevant for the calibration of satellite instruments.

We have sampled the effect of the relatively large uncertainty in the exchange-induced transition dipole moment on the computed spectra, showing that the line shape is not strongly affected. The predicted width of the spectra qualitatively agrees with experimental results of Tran *et al.*[14] and Maté *et al.*,[21] whereas the results of Drouin *et al.*[16] appear to be significantly more narrow and structured.

We have presented the line-shape theory for two distinct absorption mechanisms, where the transition dipole moment is induced by the intermolecular exchange interaction or by intramolecular spin-orbit coupling. We show that both the width and the temperature dependence of the absorption spectrum are characteristic of the underlying mechanism: The mechanism based on the exchange interaction between colliding paramagnetic molecules leads to broader absorption spectra, of which the width and intensity both increase with increasing temperature. The intramolecular spin-orbit coupling gives rise to narrower absorption spectra which do not strongly increase in intensity with increasing temperature.

In a subsequent publication,[34] we study the contributions of both mechanisms to vibronic transitions in O_2–O_2 and O_2–N_2. This unambiguously identifies of the absorption mechanism for both pairs and may have important consequences for their relative contributions to atmospheric absorption.

APPENDIX A: ANALYTICAL SUM OVER PROJECTION QUANTUM NUMBERS

In order to evaluate the spectral density, we need to calculate matrix elements of the dipole operator of the form

$$\langle \psi_A m_A \psi_B m_B \ell m_\ell E_{\rm col} | \hat{\mu}_\kappa | \psi'_A m'_A \psi'_B m'_B \ell' m'_\ell E'_{\rm col} \rangle, \tag{A1}$$

where the wavefunctions are given by Eq. (6), and for the dipole operator, we use Eq. (12). Inserting this expansion in the matrix element of the dipole operator yields

$$\begin{aligned}
&\langle \psi_A m_A \psi_B m_B \ell m_\ell E_{\rm col} | \hat{\mu}_\kappa | \psi'_A m'_A \psi'_B m'_B \ell' m'_\ell E'_{\rm col} \rangle \\
&= \frac{\left[(N_A)(N'_A)(N_B)(N'_B)(\ell)(\ell')\right]^{1/2}}{(4\pi)^3} \sum_{L_A,L_B,\lambda,L} \langle v''_A v''_B \ell E_{\rm col} | \mathcal{D}^{\psi_A,\psi_B,\psi'_A,\psi'_B}_{L_A,L_B,\lambda,L}(r_A,r_B,R) | v'_A v'_B \ell' E'_{\rm col} \rangle \\
&\times \sum_{M_A} \int\int D^{(N_A)}_{m_A,\Lambda_A}(\phi_A,\theta_A,0) D^{(L_A)*}_{M_A,\Lambda_A-\Lambda'_A}(\phi_A,\theta_A,0) D^{(N'_A)*}_{m'_A,\Lambda'_A}(\phi_A,\theta_A,0) d\cos\theta_A d\phi_A \\
&\times \sum_{M_B} \int\int D^{(N_B)}_{m_B,\Lambda_B}(\phi_B,\theta_B,0) D^{(L_B)*}_{M_B,\Lambda_B-\Lambda'_B}(\phi_B,\theta_B,0) D^{(N'_B)*}_{m'_B,\Lambda'_B}(\phi_B,\theta_B,0) d\cos\theta_B d\phi_B \\
&\times \sum_{M} \int\int C^*_{\ell,m_\ell}(\Theta,\Phi) C_{L,M}(\Theta,\Phi) C_{\ell',m'_\ell}(\Theta,\Phi) d\cos\Theta d\Phi \sum_{\mu} \langle L_A M_A L_B M_B | \lambda\mu \rangle \langle \lambda\mu L M | 1\kappa \rangle.
\end{aligned} \tag{A2}$$

Here, $|v_X\rangle$ is the vibrational wavefunction of monomer X, which implicitly does depend on the electronic state, ψ_X. A weak dependence on the rotational quantum number, N_X, may also be included.

The integrals over products of three Wigner D-matrices are given by

$$\int\int D^{(N_A)}_{m_A,k_A}(\hat{\boldsymbol{R}}) D^{(N_B)}_{m_B,k_B}(\hat{\boldsymbol{R}}) D^{(N)*}_{m,k}(\hat{\boldsymbol{R}}) d\hat{\boldsymbol{R}} = \frac{4\pi}{(N)} \langle N_A m_A N_B m_B | N m \rangle \langle N_A k_A N_B k_B | N k \rangle, \tag{A3}$$

for $k = k_A + k_B$, and the special case $k_A = k_B = k = 0$ yields the integral over three Racah normalized spherical harmonics. Using these integrals, we obtain for the dipole matrix element,

$$\begin{aligned}
&\langle \psi_A m_A \psi_B m_B \ell m_\ell E_{\rm col} | \hat{\mu}_\kappa | \psi'_A m'_A \psi'_B m'_B \ell' m'_\ell E'_{\rm col} \rangle \\
&= \left[\frac{(N'_A)(N'_B)(\ell')}{(N_A)(N_B)(\ell)}\right]^{1/2} \sum_{L_A,L_B,\lambda,L} \langle v''_A v''_B \ell E_{\rm col} | \mathcal{D}^{\psi_A,\psi_B,\psi'_A,\psi'_B}_{L_A,L_B,\lambda,L}(r_A,r_B,R) | v'_A v'_B \ell' E'_{\rm col} \rangle \\
&\times \langle N'_A, \Lambda'_A, L_A, \Lambda_A - \Lambda'_A | N_A \Lambda_A \rangle \langle N'_B, \Lambda'_B, L_B, \Lambda_B - \Lambda'_B | N_B \Lambda_B \rangle \langle \ell' 0 L 0 | \ell 0 \rangle \\
&\times \sum_{M_A,M_B,\mu,M} \langle N'_A m'_A L_A M_A | N_A m_A \rangle \langle N'_B m'_B L_B M_B | N_B m_B \rangle \langle \ell' m'_\ell L M | \ell m_\ell \rangle \langle L_A M_A L_B M_B | \lambda\mu \rangle \langle \lambda\mu L M | 1\kappa \rangle.
\end{aligned} \tag{A4}$$

Next, we consider the square of this matrix element, summed over the angular momentum projection quantum numbers, as it occurs in Eq. (2),

$$\begin{aligned}
&\sum_{m_A,m_B,m_\ell,m'_A,m'_B,m'_\ell} \left| \langle \psi_A m_A \psi_B m_B \ell m_\ell E_{\rm col} | \hat{\mu}_\kappa | \psi'_A m'_A \psi'_B m'_B \ell' m'_\ell E'_{\rm col} \rangle \right|^2 \\
&= \frac{(N'_A)(N'_B)(\ell')}{(N_A)(N_B)(\ell)} \sum_{L,L'} \langle \ell' 0 L 0 | \ell 0 \rangle \langle \ell' 0 L' 0 | \ell 0 \rangle \sum_{L_A,L_B,\lambda} \langle v''_A v''_B \ell E_{\rm col} | \mathcal{D}^{\psi_A,\psi_B,\psi'_A,\psi'_B}_{L_A,L_B,\lambda,L}(r_A,r_B,R) | v'_A v'_B \ell' E'_{\rm col} \rangle \\
&\times \langle N'_A, \Lambda'_A, L_A, \Lambda_A - \Lambda'_A | N_A \Lambda_A \rangle \langle N'_B, \Lambda'_B, L_B, \Lambda_B - \Lambda'_B | N_B \Lambda_B \rangle \sum_{L'_A,L'_B,\lambda'} \langle v''_A v''_B \ell E_{\rm col} \left| \mathcal{D}^{\psi_A,\psi_B,\psi'_A,\psi'_B}_{L'_A,L'_B,\lambda',L'}(r_A,r_B,R) \right| v'_A v'_B \ell' E'_{\rm col} \rangle^* \\
&\times \langle N'_A, \Lambda'_A, L'_A, \Lambda_A - \Lambda'_A | N_A \Lambda_A \rangle \langle N'_B, \Lambda'_B, L'_B, \Lambda_B - \Lambda'_B | N_B \Lambda_B \rangle \sum_{M_A,M_B,\mu,M} \langle L_A M_A L_B M_B | \lambda\mu \rangle \langle \lambda\mu L M | 1\kappa \rangle \\
&\times \sum_{M'_A,M'_B,\mu',M'} \langle L'_A M'_A L'_B M'_B | \lambda'\mu' \rangle \langle \lambda'\mu' L' M' | 1\kappa \rangle \sum_{m_A,m'_A} \langle N'_A m'_A L_A M_A | N_A m_A \rangle \langle N'_A m'_A L'_A M'_A | N_A m_A \rangle \\
&\times \sum_{m_B,m'_B} \langle N'_B m'_B L_B M_B | N_B m_B \rangle \langle N'_B m'_B L'_B M'_B | N_B m_B \rangle \sum_{m_\ell,m'_\ell} \langle \ell' m'_\ell L M | \ell m_\ell \rangle \langle \ell' m'_\ell L' M' | \ell m_\ell \rangle.
\end{aligned} \tag{A5}$$

We then use the orthogonality of the Clebsch-Gordan coefficients

$$\sum_{m_1,m_2} \langle N_1 m_1 N_2 m_2 | J M \rangle \langle N_1 m_1 N_2 m_2 | J' M' \rangle = \delta_{J,J'} \delta_{M,M'} \tag{A6}$$

to perform the sums over the space-fixed projection quantum numbers, which yields

$$\sum_{m_A,m_B,m_\ell,m'_A,m'_B,m'_\ell} \left|\langle \boldsymbol{\psi}_A m_A \boldsymbol{\psi}_B m_B \ell m_\ell E_{\rm col}|\hat{\mu}_\kappa|\boldsymbol{\psi}'_A m'_A \boldsymbol{\psi}'_B m'_B \ell' m'_\ell E'_{\rm col}\rangle\right|^2$$
$$= \sum_{L_A,L_B,\lambda,L} \frac{(N'_A)(N'_B)(\ell')}{(L_A)(L_B)(L)} \langle N'_A,\Lambda'_A,L_A,\Lambda_A-\Lambda'_A|N_A\Lambda_A\rangle^2 \langle N'_B,\Lambda'_B,L_B,\Lambda_B-\Lambda'_B|N_B\Lambda_B\rangle^2$$
$$\times \langle \ell' 0 L 0|\ell 0\rangle^2 \left|\langle v''_A v''_B \ell E_{\rm col}|\mathcal{D}^{\psi_A,\psi_B,\psi'_A,\psi'_B}_{L_A,L_B,\lambda,L}(r_A,r_B,R)|v'_A v'_B \ell' E'_{\rm col}\rangle\right|^2. \tag{A7}$$

Finally, we neglect the vibrational dependence of the potential, and hence the vibrational dependence of the radial wavefunctions. We further neglect the vibrational dependence of the dipole moment to obtain

$$\sum_{m_A,m_B,m_\ell,m'_A,m'_B,m'_\ell} \left|\langle \boldsymbol{\psi}_A m_A \boldsymbol{\psi}_B m_B \ell m_\ell E_{\rm col}|\hat{\mu}_\kappa|\boldsymbol{\psi}'_A m'_A \boldsymbol{\psi}'_B m'_B \ell' m'_\ell E'_{\rm col}\rangle\right|^2$$
$$= |\langle v''_A|v'_A\rangle|^2 |\langle v''_B|v'_B\rangle|^2 \sum_{L_A,L_B,\lambda,L} \frac{(N'_A)(N'_B)(\ell')}{(L_A)(L_B)(L)} \langle N'_A,\Lambda'_A,L_A,\Lambda_A-\Lambda'_A|N_A\Lambda_A\rangle^2$$
$$\times \langle N'_B,\Lambda'_B,L_B,\Lambda_B-\Lambda'_B|N_B\Lambda_B\rangle^2 \langle \ell' 0 L 0|\ell 0\rangle^2 \left|\langle \ell E_{\rm col}|\mathcal{D}^{\psi_A,\psi_B,\psi'_A,\psi'_B}_{L_A,L_B,\lambda,L}(R)|\ell' E'_{\rm col}\rangle\right|^2, \tag{A8}$$

that is, the vibrational dependence is contained completely in products of Franck-Condon factors.

APPENDIX B: SPECTRAL DENSITY FOR THE SPIN-ORBIT MECHANISM

In order to evaluate the spectral density for the spin-orbit-based mechanism, we again consider matrix elements of the form

$$\langle \boldsymbol{\psi}_A m_A \boldsymbol{\psi}_B m_B \ell m_\ell E_{\rm col}|\hat{\mu}_\kappa|\boldsymbol{\psi}'_A m'_A \boldsymbol{\psi}'_B m'_B \ell' m'_\ell E'_{\rm col}\rangle, \tag{B1}$$

where we stress that the monomer states are not implicitly spin-coupled to an overall triplet. We assume that the potential—and hence radial wavefunctions—is independent of the spin-coupling of the monomers, such that we can drop the spin quantum numbers of the perturbing monomer, molecule B. For the wavefunction of the absorbing monomer, molecule A, we substitute Eq. (25), and we use for the spin-electronic matrix element of the dipole operator, the expansion of Eq. (21). The equivalent of Eq. (A5), having neglected the vibrational dependence of the dipole moment, then becomes

$$\sum_{m_{N_A},m_{S_A},m_B,m_\ell,m'_A,m'_B,m'_\ell} \left|\langle \boldsymbol{\psi}_A m_A \boldsymbol{\psi}_B m_B \ell m_\ell E_{\rm col}|\hat{\mu}_\kappa|\boldsymbol{\psi}'_A m'_A \boldsymbol{\psi}'_B m'_B \ell' m'_\ell E'_{\rm col}\rangle\right|^2$$
$$= |\langle v''_A|v'_A\rangle|^2 |\langle v''_B|v'_B\rangle|^2 \sum_{j_A,j'_A} \frac{(N'_A)(N'_B)(\ell')}{(j_A)^{1/2}(j'_A)^{1/2}(N_B)(\ell)} \sum_{L,L'} \langle \ell' 0 L 0|\ell 0\rangle \langle \ell' 0 L' 0|\ell 0\rangle$$
$$\times \sum_{L_A,L_B,\lambda} \langle N'_A,\Lambda'_A,L_A,\Omega_A-\Lambda'_A|j_A\Omega_A\rangle \langle N'_B,\Lambda'_B,L_B,\Lambda_B-\Lambda'_B|N_B\Lambda_B\rangle$$
$$\times \sum_{L'_A,L'_B,\lambda'} \langle N'_A,\Lambda'_A,L'_A,\Omega_A-\Lambda'_A|j_A\Omega_A\rangle \langle N'_B,\Lambda'_B,L'_B,\Lambda_B-\Lambda'_B|N_B\Lambda_B\rangle \sum_{M_A,M_B,\mu,M} \langle L_A M_A L_B M_B|\lambda\mu\rangle \langle \lambda\mu L M|1\kappa\rangle$$
$$\times \sum_{M'_A,M'_B,\mu',M'} \langle L'_A M'_A L'_B M'_B|\lambda'\mu'\rangle \langle \lambda'\mu' L' M'|1\kappa\rangle \sum_{m_{j_A},m'_{j_A},m'_A} \langle N'_A m'_A L_A M_A|j_A m_{j_A}\rangle \langle N'_A m'_A L'_A M'_A|j'_A m'_{j_A}\rangle$$
$$\times \sum_{m_B,m'_B} \langle N'_B m'_B L_B M_B|N_B m_B\rangle \langle N'_B m'_B L'_B M'_B|N_B m_B\rangle \sum_{m_\ell,m'_\ell} \langle \ell' m'_\ell L M|\ell m_\ell\rangle \langle \ell' m'_\ell L' M'|\ell m_\ell\rangle$$
$$\times \sum_{\Sigma_A} \frac{(N_A)^{1/2}}{(j_A)^{1/2}} \langle N_A\Lambda_A S_A\Sigma_A|j_A\Omega_A\rangle \langle \ell E_{\rm col}|\mathcal{D}^{{\rm SO},X^3\Sigma_g^-,\Omega_A\to\psi'_A}_{L_A,L_B,\lambda,L}|\ell' E'_{\rm col}\rangle$$
$$\times \sum_{\Sigma_{A'}} \frac{(N_A)^{1/2}}{(j'_A)^{1/2}} \langle N_A\Lambda_A S_A\Sigma'_A|j'_A\Omega'_A\rangle \langle \ell E_{\rm col}|\mathcal{D}^{{\rm SO},X^3\Sigma_g^-,\Omega'_A\to\psi'_A}_{L'_A,L'_B,\lambda',L'}|\ell' E'_{\rm col}\rangle^* \sum_{m_{N_A},m_{S_A}} \langle N_A m_{N_A} S_A m_{S_A}|j_A m_{j_A}\rangle \langle N_A m_{N_A} S_A m_{S_A}|j'_A m'_{j_A}\rangle. \tag{B2}$$

The sum on the last line can be carried out using the orthogonality relation in Eq. (A6). This result closely resembles Eq. (A5), with an additional factor resulting from the transformation between Hund's case (a) and (b) bases, j_A playing the role of N_A, sums over j_A and Σ_A, and a different Σ_A-dependent dipole function. Proceeding identically as for the exchange based mechanism,

we obtain

$$\sum_{m_{N_A},m_B,m_\ell,m'_A,m'_B,m'_\ell} \left|\langle \psi_A m_A \psi_B m_B \ell m_\ell E_{\rm col}|\hat{\mu}_\kappa|\psi'_A m'_A \psi'_B m'_B \ell' m'_\ell E'_{\rm col}\rangle\right|^2$$
$$= \sum_{j_A,\Sigma_A,\Sigma_{A'}} \frac{(N_A)}{(j_A)} \langle N_A \Lambda_A S_A \Sigma_A | j_A \Omega_A\rangle \langle N_A \Lambda_A S_A \Sigma'_A | j_A \Omega'_A\rangle |\langle v''_A | v'_A\rangle|^2 |\langle v''_B | v'_B\rangle|^2$$
$$\times \sum_{L_A,L_B,\lambda,L} \frac{(N'_A)(N'_B)(\ell')}{(L_A)(L_B)(L)} \langle N'_A, \Lambda'_A, L_A, \Omega_A - \Lambda'_A | j_A \Omega_A\rangle \langle N'_A, \Lambda'_A, L_A, \Omega'_A - \Lambda'_A | j_A \Omega'_A\rangle$$
$$\times \langle \ell E_{\rm col}|\mathcal{D}^{{\rm SO},X^3\Sigma_g^-,\Omega_A\to\psi'_A}_{L_A,L_B,\lambda,L}(R)|\ell' E'_{\rm col}\rangle \langle \ell E_{\rm col}|\mathcal{D}^{{\rm SO},X^3\Sigma_g^-,\Omega'_A\to\psi'_A}_{L_A,L_B,\lambda,L}(R)|\ell' E'_{\rm col}\rangle^* \langle N'_B, \Lambda'_B, L_B, \Lambda_B - \Lambda'_B | N_B \Lambda_B\rangle^2 \langle \ell' 0 L 0 | \ell 0\rangle^2. \quad \text{(B3)}$$

In the special case where only the $\Sigma = 0$ component contributes, this simplifies to

$$\sum_{m_{N_A},m_B,m_\ell,m'_A,m'_B,m'_\ell} \left|\langle \psi_A m_A \psi_B m_B \ell m_\ell E_{\rm col}|\hat{\mu}_\kappa|\psi'_A m'_A \psi'_B m'_B \ell' m'_\ell E'_{\rm col}\rangle\right|^2$$
$$= \sum_{j_A} \frac{(N_A)}{(j_A)} \langle N_A \Lambda_A S_A 0 | j_A \Lambda_A\rangle^2 |\langle v''_A | v'_A\rangle|^2 |\langle v''_B | v'_B\rangle|^2 \sum_{L_A,L_B,\lambda,L} \frac{(N'_A)(N'_B)(\ell')}{(L_A)(L_B)(L)}$$
$$\times \langle N'_A, \Lambda'_A, L_A, \Lambda_A - \Lambda'_A | j_A \Lambda_A\rangle^2 \langle N'_B, \Lambda'_B, L_B, \Lambda_B - \Lambda'_B | N_B \Lambda_B\rangle^2 \langle \ell' 0 L 0 | \ell 0\rangle^2 \left|\langle \ell E_{\rm col}|\mathcal{D}^{{\rm SO},X^3\Sigma_g^-,0\to\psi'_A}_{L_A,L_B,\lambda,L}(R)|\ell' E'_{\rm col}\rangle\right|^2, \quad \text{(B4)}$$

which closely resembles Eq. (A8), except for the occurrence of the j_A quantum number which is summed over and which plays the role of N_A, as well as for an additional factor arising from the transformation between Hund's case (a) and (b) bases. The monomer energies are determined by the rotational quantum number N_A, not total monomer angular momentum j_A. If $\Sigma_A \neq 0$ components contribute, Eq. (B3) should be used, which contains interference terms between the different Σ_A components.

[1] A. Eldering, S. Boland, B. Solish, D. Crisp, P. Kahn, and M. Gunson, "High precision atmospheric CO2 measurements from space: The design and implementation of OCO-2," in *Aerospace Conference, 2012* (IEEE, 2012), pp. 1–10.
[2] Z. Kuang, J. S. Margolis, G. C. Toon, D. Crisp, and Y. L. Yung, Geophys. Res. Lett. **29**, 11-1, doi:10.1029/2001gl014298 (2002).
[3] C. E. Miller *et al.*, J. Geophys. Res.: Atmos. **112**, D10314, doi:10.1029/2006JD007659 (2007).
[4] D. A. Long and J. T. Hodges, J. Geophys. Res.: Atmos. **117**, D12309, doi:10.1029/2012JD017807 (2012).
[5] D. M. O'Brien, R. M. Mitchell, S. A. English, and G. A. Da Costa, J. Atmos. Oceanic Technol. **15**, 1272 (1998).
[6] B. van Diedenhoven, O. P. Hasekamp, and I. Aben, Atmos. Chem. Phys. **5**, 2109 (2005).
[7] B. van Diedenhoven, O. P. Hasekamp, and J. Landgraf, J. Geophys. Res. **112**, D15208, doi:10.1029/2006JD008155 (2007).
[8] J.-M. Hartmann, C. Boulet, and D. Robert, *Collisional Effects on Molecular Spectra* (Elsevier, 2008).
[9] B. Minaev, O. Vahtras, and H. Ågren, Chem. Phys. **208**, 299 (1996).
[10] B. Minaev, J. Mol. Struct.: THEOCHEM **183**, 207 (1989).
[11] B. F. Minaev, Russ. Chem. Rev. **76**, 1059 (2007).
[12] B. F. Minaev, Int. J. Quantum Chem. **17**, 367 (1980).
[13] I. E. Gordon, S. Kassi, A. Campargue, and G. C. Toon, J. Quant. Spectrosc. Radiat. Transfer **111**, 1174 (2010).
[14] H. Tran, C. Boulet, and J.-M. Hartmann, J. Geophys. Res. **111**, D15210, doi:10.1029/2005JD006869 (2006).
[15] D. L. A. G. Grimminck, F. R. Spiering, L. M. C. Janssen, A. van der Avoird, W. J. van der Zande, and G. C. Groenenboom, J. Chem. Phys. **140**, 204314 (2014).
[16] B. J. Drouin *et al.*, J. Quant. Spectrosc. Radiat. Transfer **186**, 118 (2017).
[17] G. C. Tabisz, E. J. Allin, and H. L. Welsh, Can. J. Phys. **47**, 2859 (1969).
[18] F. R. Spiering, M. B. Kiseleva, N. N. Filippov, H. Naus, B. van Lieshout, C. Weijenborg, and W. J. van der Zande, J. Chem. Phys. **133**, 114305 (2010).
[19] D. A. Long, D. J. Robichaud, and J. T. Hodges, J. Chem. Phys. **137**, 014307 (2012).
[20] M. V. Tonkov, N. N. Filippov, Y. M. Timofeyev, and A. V. Polyakov, J. Quant. Spectrosc. Radiat. Transfer **56**, 783 (1996).
[21] B. Maté, C. Lugez, G. T. Fraser, and W. J. Lafferty, J. Geophys. Res.: Atmos. **104**, 30585, doi:10.1029/1999jd900824 (1999).
[22] A. R. W. McKellar, N. H. Rich, and H. L. Welsh, Can. J. Phys. **50**, 1 (1972).
[23] T. Karman, A. van der Avoird, and G. C. Groenenboom, J. Chem. Phys. **147**, 084306 (2017).
[24] T. Karman, E. Miliordos, K. L. C. Hunt, G. C. Groenenboom, and A. van der Avoird, J. Chem. Phys. **142**, 084306 (2015).
[25] T. Karman, A. van der Avoird, and G. C. Groenenboom, J. Chem. Phys. **142**, 084305 (2015).
[26] M. Abramowitz and I. A. Stegun, *Handbook of Mathematical Functions* (National Bureau of Standards, Washington, DC, 1964).
[27] G. Moreau, J. Boissoles, C. Boulet, R. Tipping, and Q. Ma, J. Quant. Spectrosc. Radiat. Transfer **64**, 87 (2000).
[28] B. F. Minaev, Chem. Phys. **252**, 25 (2000).
[29] D. A. Long, D. K. Havey, M. Okumura, H. M. Pickett, C. E. Miller, and J. T. Hodges, Phys. Rev. A **80**, 042513 (2009).
[30] T. K. Balasubramanian and O. Narayanan, Acta Phys. Hung. **74**, 341 (1994).
[31] T. K. Balasubramanian and A. P. Mishra, Phys. Rev. A **84**, 056501 (2011).
[32] G. Breit and E. Wigner, Phys. Rev. **49**, 519 (1936).
[33] R. Nichols, J. Res. Natl. Bur. Stand., Sect. A **69**, 369 (1965).
[34] T. Karman, M. A. J. Koenis, A. Banerjee, D. H. Parker, I. E. Gordon, A. van der Avoird, W. J. van der Zande, and G. C. Groenenboom, "Mechanisms of collision-induced absorption for spin-forbidden transitions" (unpublished).